# Effect of Interfacial Properties on the Clustering of Alumina Inclusions in Molten Iron

Lichun ZHENG*, Annelies MALFLIET, Patrick WOLLANTS, Bart BLANPAIN, Muxing GUO

(Department of Materials Engineering, KU Leuven, Kasteelpark Arenberg 44 box 2450, 3001 Leuven, Belgium)

*Corresponding author: e-mail: zg.lichun@gmail.com

**Abstract:** Clustering of alumina inclusions in liquid steel commonly takes place during Al deoxidization process and the extent of clustering significantly influences steel cleanliness. The clustering is suggested to have a close relationship with the interfacial properties of alumina inclusions and liquid steel. In the present work, the effect of the interfacial properties on the clustering of alumina inclusions was investigated. Different amounts of Te were added to molten iron before Al deoxidization at 1873K to modify the interfacial properties. A method was developed to analyze alumina clustering, such as the mean diameter, the clustering degree and the average number of particles per cluster. The values of these parameters were found to increase with increasing Te addition up to 200ppm, thereafter to decrease with further Te addition. The effect of Te addition on the clustering of alumina inclusions is discussed with the theory of spontaneous cavitation between non-wetting surfaces. Te affects the clustering in two opposite ways. First, it decreases the surface tension of molten iron. This makes clustering less likely; Second, it makes alumina inclusions more faceted. This favors clustering. Due to the two opposite effects, the extent of alumina clustering reaches a maximum at 200ppm Te addition.

**Keywords:** alumina inclusions, molten iron, interfacial properties, clustering

## 1 Introduction

As non-metallic inclusions can deteriorate steel mechanical properties[1,2], their maximum size is restricted in many steel grades[3]. Growth by turbulent collision can strongly increase inclusion size due to collision and agglomeration of inclusions, i.e. clustering[4]. Due to their large size, clusters can float up more easily to the slag phase. They are, however, very bad to steel properties if they remain in solidified steel.

Clustering of non-metallic inclusions in liquid steel, especially of alumina inclusions, has long been known[4]. Clustering was found to occur mainly among non-metallic inclusions that can't be wetted by liquid steel, indicating the existence of a strong attractive force between the inclusions. With confocal scanning laser microscopy (CSLM), the clustering of non-metallic inclusions on the surface of liquid steel has been well understood. Un-wetted inclusions are observed to move to each other, followed by collision and agglomeration[5,6]. The attraction is considered to arise from capillary force[7]. However, understanding of clustering between un-wetted inclusions in the bulk of liquid steel is still quite limited, such as the origin of attraction, its magnitude and range. Clustering of non-metallic inclusions in liquid steel is suggested to have a close relationship with the interfacial properties of inclusions and liquid steel, such as the wettability, the surface tension of liquid steel and the interfacial energy[4, 8-10].

The purpose of this study is to clarify the effect of interfacial properties on the clustering of alumina inclusions. To modify the interfacial properties of alumina inclusions and molten iron, different amounts of surfactant tellurium (Te) were added to the molten iron before Al deoxidization. The extent of clustering of alumina inclusions was characterized and effect of Te addition on the clustering is discussed.

## 2 Experimental Methods

### 2.1 Procedure

The experiments were carried out in a vertical tube furnace (heating element $MoSi_2$) under purified Ar atmosphere (0.5L/min). 80g of electrolytic iron, together with reagent grade $Fe_2O_3$ powder used to adjust the initial oxygen content, was melted in a magnesia crucible (27mm ID and 50mm H) at 1873K. After stabilizing for 30 min, Te was added into the molten iron through a quartz tube (8mm ID). Immediately, the melt was stirred for 30s with an alumina rod. 3 min later, 0.12g Al was added in the same way as the Te, followed by stirring for 30s with the alumina rod. The melt was held for 1, 3, and 10 min at 1873K after Al addition. Thereafter, iron samples were taken with a quartz tube (6mm ID), and rapidly quenched in water. Sampling was always done close to the crucible bottom. Table 1 shows an overview of the experimental conditions.

**Table 1 Details of the experimental conditions**

| Test No. | O addition/ppm | Te addition/ppm |
|---|---|---|
| H1 | 400 | 0 |
| H2 | | 40 |
| H3 | | 200 |
| H4 | | 1000 |

### 2.2 Chemical Analysis

The content of total oxygen in the iron samples was measured with a LECO combustion analyzer using the inert gas fusion method. The soluble Al and total Te contents were analyzed with inductively coupled plasma atomic emission spectroscopy (ICP-AES).

### 2.3 Inclusion Characterization

(1) Inclusion Size. To measure the planar size of alumina inclusions in a polished cross section of iron samples, successive microphotographs were taken with a high resolution SEM (Philips XL 30) at 1000×. Then the photographs were processed with an image analyzer to obtain the number, size (equivalent diameter $d_A^i$) and centroid coordinates ($x$,$y$) of the inclusions. During the measurements, clustered inclusions were automatically split into several discrete inclusions with the Watershed separation technique available in the software. Alumina clusters were reconstructed as described in the following section.

(2) Cluster Construction. Alumina clusters usually appears as a group of discrete particles in a cross section[4]. The following method was developed by the authors to construct 2D alumina clusters. To determine whether two discrete particles might adhere to each other in 3D, a critical inter-particle distance $h_0$ is defined in Eq.(1).

The construction starts with a single particle numbered $p_i$. All its neighboring particles with inter-particle distances smaller than $h_0$ are identified. The particle $p_i$, together with these neighboring particles, is called cluster $c_i$. The construction continues with next particle in the cluster $c_i$ numbered $p_j$. All its neighboring particles (outside cluster $c_i$) with inter-particle distances smaller than $h_0$ are also identified and added to the cluster $c_i$. This step is repeated with every particle in the cluster $c_i$ until any particle outside the cluster $c_i$ has inter-particle distances relative to any particles inside the cluster $c_i$ larger than $h_0$. The construction is performed by programming with MATLAB software.

$$h_0 = \bar{d}_v - \bar{d}_A \tag{1}$$

$$\bar{d}_v = \frac{\pi}{2} \cdot n / \sum_{i=1}^{n} (1/d_A^i) \tag{2}$$

where $h_0$ is the critical inter-particle distance, $\bar{d}_A$ $\bar{d}_A$ and $\bar{d}_V$ are the mean planar and mean spatial diameter of the particles[11], and $d_A^i$ is the equivalent planar diameter of particle i.

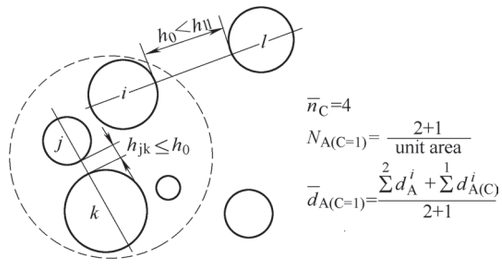


**Fig.1 Construction of an alumina cluster and a corresponding example of symbols used for characterizing alumina inclusions**

With this method, some parameters can be obtained to characterize alumina clustering, such as clustering degree $C_D$, defined as the ratio of the number of clustered particles to the total number of particles and average number of particles per cluster $\bar{n}_C$. Also, we can obtain the equivalent diameter $d_{A(C)}^i$ of each cluster and the number density $N_{A(C=1)}$ of alumina inclusions (particles and clusters). For the symbols of $\bar{n}_C$, $\bar{d}_{A(c=1)}$ and $N_{A(C=1)}$, an example is shown in Fig.1.

## 3 Results and Discussion

Table 2 shows the experimental results. Based on data from literature[12, 13], the effect of Te and O on the interfacial properties of alumina inclusions and molten iron is summarized and shown in Fig.2.

### 3.1 Inclusion Size

Te was found to have a strong effect on the mean diameter $\bar{d}_{A(c=1)}$ of alumina inclusions. The results are shown in Fig.3 as a function of holding time. The error bars represent the standard deviation. The $\bar{d}_{A(c=1)}$ increase slightly with the holding time for tests H1, H2

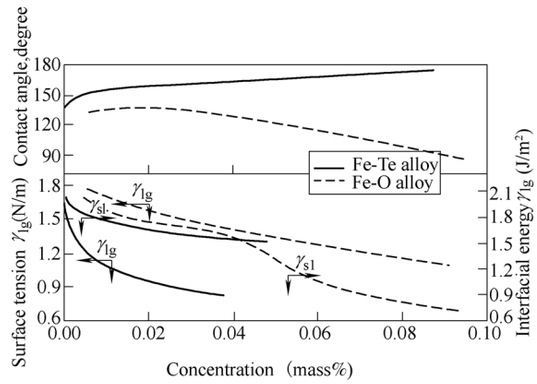


**Fig. 2 Effect of O and Te on the interfacial properties of alumina inclusions and molten iron at 1873K[12, 13]**

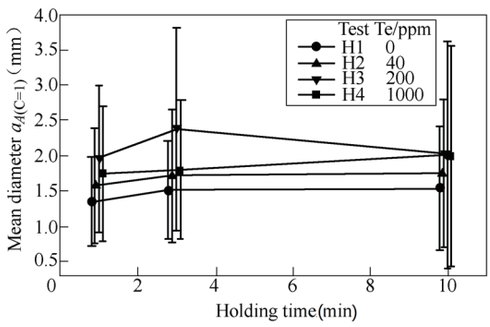


**Fig.3 Effect of Te addition on the mean diameter of alumina inclusions**

and H4, with respective Te additions of 0, 40 and 1000 ppm. For test H3 with Te addition of 200ppm, $\bar{d}_{A(c=1)}$ increases from 1 to 3 min and thereafter decreases with increasing holding time. Moreover, for a given holding time, $\bar{d}_{A(c=1)}$ increases with increasing Te addition up to 200 ppm, and then decreases with further Te addition.

As alumina growth by collision dominates under the condition of turbulence[4, 14, 15], we conclude that Te promotes alumina growth by collision. This effect is strongly linked to the amount of Te.

### 3.2 Clustering Degree

Te addition increases clustering tendency, as shown in Fig.4. The error bars represent the variation of measured $C_D$ values when fluctuating the critical values h in the range of $0.8h_0$ to $1.2h_0$. The variation of $C_D$ values for most samples is within 2% when

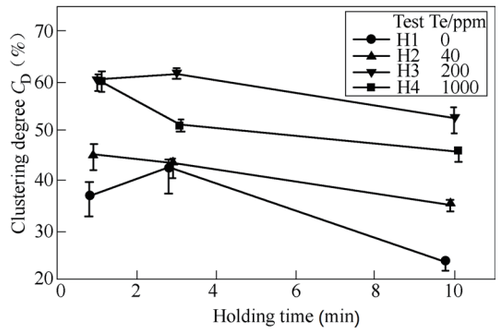


**Fig.4 Effect of Te addition on the alumina clustering degree**

**Table 2 Characteristics of alumina inclusions and chemical analysis of the iron samples**

| Sample No. | Holding Time | $\bar{d}_{A(c=1)}$ | $N_{A(C=1)}$ | T.O | Sol.Al | T.Te |
|---|---|---|---|---|---|---|
| | ( min) | (μm) | ($mm^{-2}$) | (mass ppm) | | |
| H1-1 | 1 | 1.35 | 458 | 190 | 1019 | - |
| H1-2 | 3 | 1.52 | 305 | 160 | 1071 | - |
| H1-3 | 10 | 1.54 | 194 | 95 | 1005 | - |
| H2-1 | 1 | 1.58 | 292 | 180 | 890 | 28 |
| H2-2 | 3 | 1.72 | 229 | 150 | 878 | 21 |
| H2-3 | 10 | 1.75 | 146 | 120 | 835 | 15 |
| H3-1 | 1 | 1.96 | 287 | 220 | 855 | 206 |
| H3-2 | 3 | 2.38 | 171 | 180 | 825 | 213 |
| H3-3 | 10 | 2.02 | 100 | 100 | 795 | 180 |
| H4-1 | 1 | 1.74 | 274 | 240 | 940 | 884 |
| H4-2 | 3 | 1.80 | 216 | 198 | 931 | 869 |
| H4-3 | 10 | 2.00 | 111 | 110 | 950 | 745 |

increasing the critical value $h$ from $h_0$ to $1.2h_0$, which indicates a high accuracy of the measured $C_D$ values.

The $C_D$ values for all the tests show a downward trend with increasing holding time. This could be explained by the floating up of the larger clusters. Moreover, for a given holding time, the $C_D$ values increase with increasing Te addition up to 200ppm, and then decrease with further Te addition.

We conclude that Te addition probably triggers two mechanisms of clustering: one that favors clustering and one that makes clustering less likely.

### 3.3 Average Number of Particles per Cluster

The average number of particles per cluster $\bar{n}_C$ was calculated and shown in Fig.5. The error bars

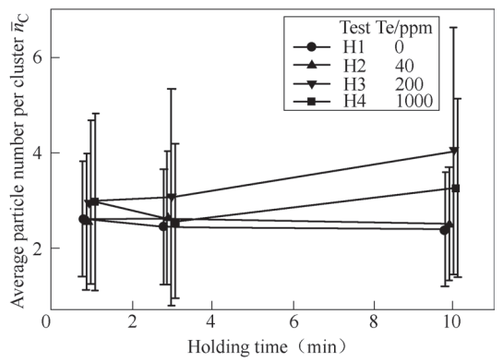


**Fig. 5 Effect of Te addition on the average number of particles per cluster**

show the corresponding arithmetic standard deviation. For tests H1 and H2, $\bar{n}_C$ roughly stays constant around 2.5 during the holding time. Thus, the addition of 40ppm Te has no measurable effect on $\bar{n}_C$. When 200ppm is added in test H3, $\bar{n}_C$ increases from 3.0 at 1 min to 4.0 at 10 min. Further increasing Te addition to 1000ppm decreases $\bar{n}_C$ considerably below the values of test H3 with 200ppm Te addition.

### 3.4 Mechanism of Inclusion Clustering

The interaction between particles in non-wetting solutions has been extensively studied[16]. Measurements of these interactions have revealed the existence of strong attractions of much longer range than the classical van der Waals force[16-18]. To account for the strong attractions, the proposal that in non-wetting solutions the liquid may be spontaneously expelled from the gap between two approaching particles to form a gas cavity, as shown in Fig.6, is the most attractive and has been validated by many experiments[19-21]. Therefore, the effect of Te addition on the clustering of alumina inclusions will be discussed based on this mechanism.

The formation of a gas cavity is thermodynamically favorable in non-wetting solutions, as seen from Eq.(3). Once the gas cavity is formed, there will be an attractive force between two surfaces. This attractive force is the sum of the surface tension force and the force that results from the pressure drop across the liquid-gas interface, as shown in Eq.(4) [22, 23].

$$\gamma_{sg} - \gamma_{sl} = \gamma_{lg} \cdot \cos\theta \tag{3}$$

$$F = 2\pi\gamma_{lg} l - \pi l^2 \Delta\rho \tag{4}$$

$$\Delta P = P_i - P_o \tag{5}$$

where $F$ is the attractive force, $P_i$ is the pressure in the gas cavity, $P_o$ is the pressure in the liquid, $l$ and $r$ are the principle radii of the gas cavity (Fig.6).

To calculate the attractive force between two particles, the principle radii $l$ and $r$, i.e. the equilibrium shape of the cavity, should be determined first. Methods of optimizing the shape of the cavity confined by two identical spheres have been available in literature[18, 23, 24]. In the present study, we focus on how interfacial properties and particle shapes affect the attractive force $F$. The shape of the liquid-gas interface is described by a piece of a circle with radius $r$, as shown in Fig.6. Then, the principle radii $l$ and $r$ can be expressed as functions of the filling angle $\alpha$. As the contact types of two particles are various in practice, here we only consider three general cases, i.e. sphere and sphere (S-S), sphere and plate (S-P), and plate and plate (P-P). The principle radii l and r are derived and listed in Table 3.

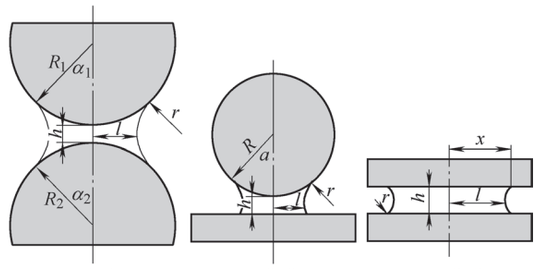


(a) S–S (b) S–P (c) P–P

**Fig. 6 Basic geometry of the gas cavity of different contact types**

The equilibrium shape of the cavity can be determined by minimizing its Gibbs free energy of formation[24]. For a gas cavity, the Gibbs free energy is expressed as[18]:

$$G = P_o V - N k_B T \ln V + \gamma_{lg} A_{lg} + (\gamma_{sg} - \gamma_{sl}) \cdot A_{sl} \tag{6}$$

where $V$ is the volume of the gas cavity, $N$ is thenumber of gas molecules, $A_{lg}$ is the liquid-gas interfacial area and $A_{sl}$ is the solid-liquid interfacial area.

Expressing $V$, $A_{lg}$ and $A_{sl}$ as functions of the filling angle $\alpha$, the equilibrium value of $\alpha$ can be obtained from $dG = f(a) = 0$. Then the attractive force $F$ could be calculated.

Values of parameters and interfacial propertiesused in the calculation are listed in Table 4 and 5.

The calculated attractive force as a function of

**Table 3 Calculated principle radii of gas cavity for different contact types**

| Contact type | Principle radii | |
|---|---|---|
| | $r$ | $l$ |
| S-S | $r = -\dfrac{R_1(1-\cos\alpha_1) + R2(1-\cos\alpha_2) + H}{\cos(\theta-\alpha_1) + \cos(\theta+\alpha_2)}$ | $l = R_1 \sin\alpha_1 - r[1-\sin(\theta-\alpha_1)]$ |
| S-P[25] | $r = -\dfrac{R(1-\cos\alpha) + H}{\cos(\theta-\alpha) + \cos(\theta)}$ | $l = R\sin\alpha - r[1-\sin(\theta-\alpha)]$ |
| P-P[18] | $r = -\dfrac{H}{2\cos(\theta)}$ | $l = x - r(1-\sin\theta]$ |

Note: $R$, $R_1$ and $R_2$ are the radii of particles; $\alpha$, $\alpha_1$ and $\alpha_2$ are the filling angles; $H$ is the separation distance between the two particles; $x$ is the radius of the gas cavity (Fig.6).

**Table 4 Parameters used in the calculation**

| Parameters | Values |
|---|---|
| Radius of sphere / μm | 10 |
| Radius of plate (round) / μm | 10 |
| Number of gas molecules $N$ | 0 |
| Pressure outside the cavity $P_o$ / atm | 1 |
| Pressure inside the cavity $P_i$ / atm | 0 |

**Table 5 The interfacial properties used in the calculation[13]**

| Te addition | $\theta$ | $\gamma_{sl}$ | $\gamma_{lg}$ | $\gamma_{sg}$ |
|---|---|---|---|---|
| ppm | ° | $J \cdot m^{-2}$ | $N \cdot m^{-1}$ | |
| 0 | 139 | 2.11 | 1.80 | 0.75 |
| 40 | 150 | 1.88 | 1.31 | |
| 200 | 159 | 1.72 | 1.04 | |
| 1000 | 178 | 1.52 | 0.77 | |

the separation distance $H$ is shown in Fig.7. The P-P type has the largest attractive force and the longest separation distance; While the S-S type has the smallest attractive force and the shortest separation distance. This implies that faceted inclusions should form clusters most easily. This conclusion can be confirmed by literature[4]. In the present study, we also observed such a phenomenon. Fig.9 illustrates that faceted inclusions tend to form clusters while spherical inclusions tend to exist independently.

The area under the force-separation distance curve is a measure for the energy required to rupture the gas cavity. Effect of Te addition on the rupture energy for different contact types is shown in Fig.8. For all contact types, the rupture energy shows a downward trend with increasing Te addition. This is because that the attractive force is surface tension related (Eq.(4)) and that the surface tension of molten iron decreases with increasing Te content (Fig.2). Therefore, we conclude that Te addition can weaken the clustering of alumina inclusions by decreasing the surface tension of molten iron.

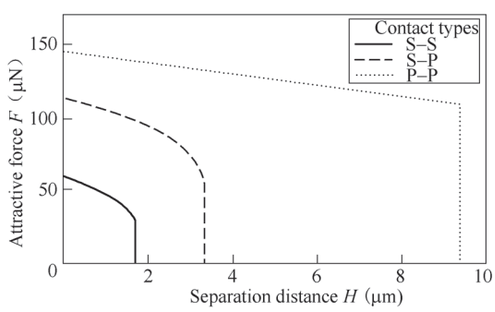


**Fig.7 Variation of attractive forces with separation distance for different contact types**

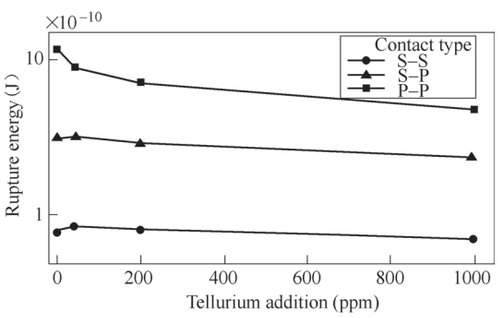


**Fig. 8 Effect of Te addition on the rupture energy of different contact types**

Based on these theoretical considerations, for the tests H1 to H4, the values of the mean diameter $\overline{d}_{A(c=1)}$, the clustering degree $C_D$ and the average number of particles per cluster $\overline{n_c}$ should follow a downward trend with increasing amounts of Te addition. However, these values increase with Te addition up to 200ppm and thereafter decrease. In order to account for this phenomenon, morphology modification of alumina inclusions due to Te addition should be considered as clustering is particle shape dependent.

Modification of crystal habits grown from solution with impurity present has been reported in a vast number of papers[26]. For example, plate-like alumina inclusions in liquid steel are suggested to be the result of adsorption of impurities on the (111) face[27]. In the present tests, we observed that the morphology of alumina inclusions changes to be more faceted even plate-like when Te is added (Fig.9).

In summary, Te addition affects alumina clustering in two ways. First, it decreases the surface tension of the molten iron (effect I); Second, it makes alumina inclusions more faceted (effect Π). According to theoretical calculations, effects of the two factors on alumina clustering are opposite. Decreasing the surface tension of molten iron weakens alumina clustering while changing alumina morphology to be more faceted strengthens the clustering. Due to the two opposite effects, the maximum values of the above mentioned parameters appear at 200ppm Te addition.

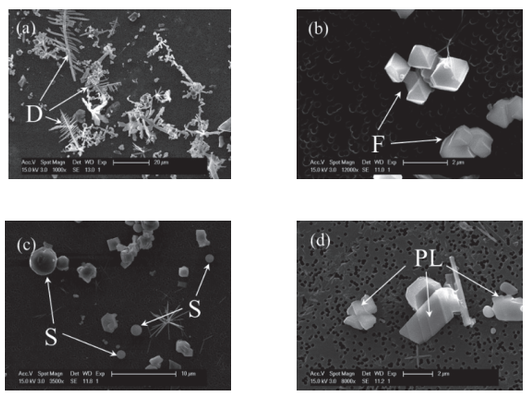


**Fig. 9 SEM images of alumina inclusions after acid extraction: (a) sample H1-1 (0 ppm Te), (b) sample H2-1 (40 ppm Te), (c) sample H3-1 (200 ppm Te), (d) sample H4-1 (1000 ppm Te). [S]: spherical; [D] dendrite; [F]: faceted; [PL]: plate-like**

## 5 Conclusions

(1) The values of the mean diameter of alumina inclusions $\bar{d}_{A(c=1)}$, the clustering degree $C_D$ and the average number of particles per cluster $\bar{n}_c$ increase with increasing Te addition up to 200ppm, thereafter, to decrease with further Te addition. The effect of Te addition on the clustering of alumina inclusions was discussed based on the cavitation theory.

(2) Theoretical calculations show that: i) faceted particles form clusters most easily. ii) decreasing the surface tension of molten iron can weaken the clustering of alumina inclusions.

(3) Te addition not only decreases the surface tension of the molten iron but also makes alumina inclusions more faceted. Effects of the two factors on alumina clustering are opposite. As a result, the maximum values of the above mentioned parameters appear at 200ppm Te addition.

## References


[1] Nicholson A, Gladman T. Non-Metallic Inclusions and Developments in Secondary Steelmaking[J]. Ironmaking Steelmaking, 1986, 13(2): 53-69.

[2] Atkinson H V, Shi G. Characterization of Inclusions in Clean Steels: A Review Including the Statistics of Extremes Methods[J]. Progress in Materials Science, 2003, 48(5): 457-520.

[3] Li S X. Effects of Inclusions on Very High Cycle Fatigue Properties of High Strength Steels[J]. Int Mater Rev, 2012, 57(2): 92-114.

[4] Braun T, Elliott J, Flemings M. The Clustering of Alumina Inclusions[J]. Metall Trans B, 1979, 10(2): 171-184.

[5] Kang Y, Sahebkar B, Scheller P R, et al. Observation on Physical Growth of Nonmetallic Inclusion in Liquid Steel During Ladle Treatment[J]. Metall Mater Trans B, 2011, 42(3): 522-534.

[6] Yin H B, Shibata H, Emi T, et al. Characteristics of Agglomeration of Various Inclusion Particles on Molten Steel Surface[J]. ISIJ Int, 1997, 37(10): 946-955.

[7] Kralchevsky P A, Nagayama K. Capillary Interactions between Particles Bound to Interfaces, Liquid Films and Biomembranes[J]. Adv Colloid Interface Sci, 2000, 85(2-3): 145-192.

[8] Nakamoto M, Tanaka T, Suzuki M, et al. Effects of Interfacial Properties between Molten Iron and Alumina on Neck Growth of Alumina Balls at Sintering in Molten Iron[J]. ISIJ Int, 2014, 54(6): 1195-1203.

[9] Cournil M, Gruy F, Gardin P, et al. Modelling of Solid Particle Aggregation Dynamics in Non-Wetting Liquid Medium[J]. Chem Eng Process, 2006, 45(7): 586-597.

[10] Kozakevi.P, Olette M. Role of Surface Phenomena in Mechanism Used for Eliminating Solid Inclusions[J]. Revue De Metallurgie, 1971, 68(10): 635-646.

[11] Ohta H, Suito H. Characteristics of Particle Size Distribution of Deoxidation Products with Mg, Zr, Al, Ca, Si/Mn and Mg/Al in Fe-10mass%Ni Alloy[J]. ISIJ Int, 2006, 46(1): 14-21.

[12] Nogi K, Ogino K. Role of Interfacial Phenomena in Deoxidation Process of Molten Iron[J]. Can Metall Q, 1983, 22(1): 19-28.

[13] Ogino K, Nogi K, Yamase O. Effects of Selenium and Tellurium on the Surface Tension of Molten Iron and the Wettability of Alumina by Molten Iron[J]. Trans ISIJ, 1983, 23(3): 234-239.

[14] Sheng D Y, Soder M, Jonsson P, et al. Modeling Micro-Inclusion Growth and Separation in Gas-Stirred Ladles[J]. Scand J Metall, 2002, 31(2): 134-147.

[15] Lei H, He J C. A Dynamic Model of Alumina Inclusion Collision Growth in the Continuous Caster[J]. J Non-Cryst Solids, 2006, 352(36-37): 3772-3780.

[16] Christenson H K, Claesson P M. Direct Measurements of the Force between Hydrophobic Surfaces in Water[J]. Adv Colloid Interface Sci, 2001, 91(3): 391-436.

[17] Israelachvili J, Pashley R. The Hydrophobic Interaction Is Long Range, Decaying Exponentially with Distance[J]. Nature, 1982, 300(5890): 341-342.

[18] Parker J L, Claesson P M, Attard P. Bubbles, Cavities, and the Long-Ranged Attraction between Hydrophobic Surfaces[J]. J Phys Chem, 1994, 98(34): 8468-8480.

[19] Christenson H K, Claesson P M. Cavitation and the Interaction between Macroscopic Hydrophobic Surfaces [J]. Science, 1988, 239(4838): 390-392.

[20] Pashley R M, Mcguiggan P M, Ninham B W, et al. Attractive Forces between Uncharged Hydrophobic Surfaces: Direct Measurements in Aqueous Solution[J]. Science, 1985, 229(4718): 1088-1089.

[21] Wood J, Sharma R. How Long Is the Long-Range Hydrophobic Attraction[J]. Langmuir, 1995, 11(12): 4797-4802.

[22] Yaminsky V V, Yushchenko V S, Amelina E A, et al. Cavity Formation Due to a Contact between Particles in a Nonwetting Liquid[J]. J Colloid Interface Sci, 1983, 96(2): 301-306.

[23] Yushchenko V S, Yaminsky V V, Shchukin E D. Interaction between Particles in a Nonwetting Liquid[J]. J Colloid Interface Sci, 1983, 96(2): 307-314.

[24] Attard P. Thermodynamic Analysis of Bridging Bubbles and a Quantitative Comparison with the Measured Hydrophobic Attraction[J]. Langmuir, 2000, 16(10): 4455-4466.

[25] Hampton M A, Nguyen A V. Systematically Altering the Hydrophobic Nanobubble Bridging Capillary Force from Attractive to Repulsive[J]. J Colloid Interface Sci, 2009, 333(2): 800-806.

[26] Sangwal K. Effects of Impurities on Crystal Growth Processes[J]. Prog Cryst Growth Charact Mater, 1996, 32(1-3): 3-43.

[27] Dekkers R, Blanpain B, Wollants P. Crystal Growth in Liquid Steel During Secondary Metallurgy[J]. Metall Mater Trans B, 2003, 34(2): 161-171.